OPTICAL AND UV-VIS LUMINESCENCE SPECTRA OF $Ni_{1-x}Zn_xFe_2O_4$ FERRITE NANOPOWDERS

A.A. SADIGOVA, Sh.N. ALIYEVA, Sh.A. AHMADOVA, I.F. YUSIBOVA, T.G. NAGHIYEV, T.R. MEHDIYEV

G.M. Abdullayev Institute of Physics of NASA,
Azerbaijan AZ-1143, Baku, H. Javid ave., 131

The optical and UV-VIS luminescent spectra of $Ni_{1-x}Zn_xFe_2O_4$ ferrite nanopowders with x = 0;0,25;0,4;0,5;0,6;0,75;1,0 were investigated in 4000-50 cm^{-1} and 200-700 nm at room temperature. The features of the diffuse reflectance spectra of $Ni_{1-x}Zn_xFe_2O_4$ ferrites were analyzed by the Kramers- Kronig procedure. The agreement with the data of published studies of other authors allowed us to give a hypothetical interpretation of the results.

Keywords: ferrites, nanopowders, IR spectra.
PACS: 41.20 Gz; 42.72 Ai

1. INTRODUCTION

$Ni_{1-x}Zn_xFe_2O_4$ is compositions of d-elements which allow to create new types elements for modern nanoelectronics. Well known the practical applications of their as magnetic cores, antennas, memory elements, microwave components, etc. The peculiarities of these ferrites is related their the crystal of structure with the formula $(Zn^{2+}{}_xFe^{3+}{}_x)[Ni^{2+}{}_{1-x}Fe^{3+}{}_{2-x}]O_4$ (x is the degree of inversion) which allow us to define their as mixed spinels. From peculiarities building of crystal structure of these spinels follow the existence superexchange interaction investigation of which define our interest to these ferrites. Earlier in [1-4] were published the results investigations of EPR, Raman, IR and etc. spectra. In this publication we presented results of optical and luminescent investigations nanopowders $Ni_{1-x}Zn_xFe_2O_4$. The luminescent spectra were excited by different wavelength from of xenon source and YAG Nd- laser.

2. SAMPLES PREPARATION

$Ni_{1-x}Zn_xFe_2O_4$ synthesized by high-temperature method with high purity components and annealing 2 hours at 960^0C [3,5]. The size of particles is from 20nm to 40 nm. The quality of nanopowders was monitored by X-ray diffractograms and optical methods. It is shown that lattice distortions resulting from deviation from stoichiometry have small effect on Raman spectra. Detailed X-ray studies of the formation of $Ni_{1-x}Zn_xFe_2O_4$ ferrite films have shown that the process of their formation, as pointed in [5], goes through three stages: at the first stage $ZnFe_2O_4$ is obtained, while part of NiO and Fe_2O_3 remain in the free state; in second stage the process of including Ni^{2+} ions in the $ZnFe_2O_4$ lattice begins and compound with an excess of Ni is formed against stoichiometry; in the third stage the composition is finally formed. The observed changes were in good agreement with concentration of Fe^{3+} cations [5] in the $Ni_{1-x}Zn_xFe_2O_4$ films. We note that it was established in [6] that the most homogeneous composition of $ZnFe_2O_4$ is achieved when using α-Fe_2O_3, A significantly smaller concentration of Fe is included into the ZnO in samples obtained when using FeO and Fe_3O_4. The spatial symmetry group of $Ni_{1-x}Zn_xFe_2O_4$, corresponded to $Fd\bar{3}m$.

3. DETAILS OF EXPERIMENTS

Optical spectra of $Ni_{1-x}Zn_xFe_2O_4$ (x=0;0,25;0,4;0,5;0,6;0,75;1,0) compositions are studied on infrared Fourier-spectrometer Vertex-70V (Bruker, Germany) with attachment of diffuse reflection in vacuum camera in spectral range from 4000cm^{-1} up to 50cm^{-1}, the standard spectral resolution is better than 0,5cm^{-1} [2, 3]. The luminescence spectra of synthesized $Ni_{1-x}Zn_xFe_2O_4$ ferrite nanopowders were studied on LS-55 spectrometer with a Monk-Giddison monochromator at 300C in the 300-700nm range. The luminescent spectra excited with wavelengths: 280 nm, 290 nm, 300 nm, 325 nm, 350 nm, 375 nm, 400 nm, 425 nm from the xenon source. The luminescent spectra of $Ni_{1-x}Zn_xFe_2O_4$ compositions were also investigated on the Confocal Raman Spectrometer with of radiation 3D Confocal Laser Microspectroscopy System Nanofinder 30 (Tokyo Instruments, Japan). The YAG Nd- laser is generate radiation 53 nm) with power from 0.1 mW to 10 mW [1].

4. EXPERIMENTAL RESULTS AND THEIR DISCUSSION

4.1 EXPERIMENTAL RESULTS OF OPTICAL INVESTIGATIONS

The infrared spectra of all studied ferrite $Ni_{1-x}Zn_xFe_2O_4$ compositions are shown in fig. 1-2. The absorption maxima and fine structures in the region from 4000cm^{-1} to 50cm^{-1} spectra were established as a result of repeated experiments and are shown in Table 1, which allows to identify the positions of genetically related spectral lines in different $Ni_{1-x}Zn_xFe_2O_4$ compositions, consistent with the results of [7,8]. When analyzing the obtained spectra, it was found that their profiles have a complex structure and when changing the composition of the composition (see table 1), not only a shift is noticeable, but also splitting into spectral components. The temperature in all the studies was equal to 300K.

131 H.Javid ave, AZ-1143
ANAS, G.M. Abdullayev Institute of Physics
E-mail: jophphysics@gmail.com

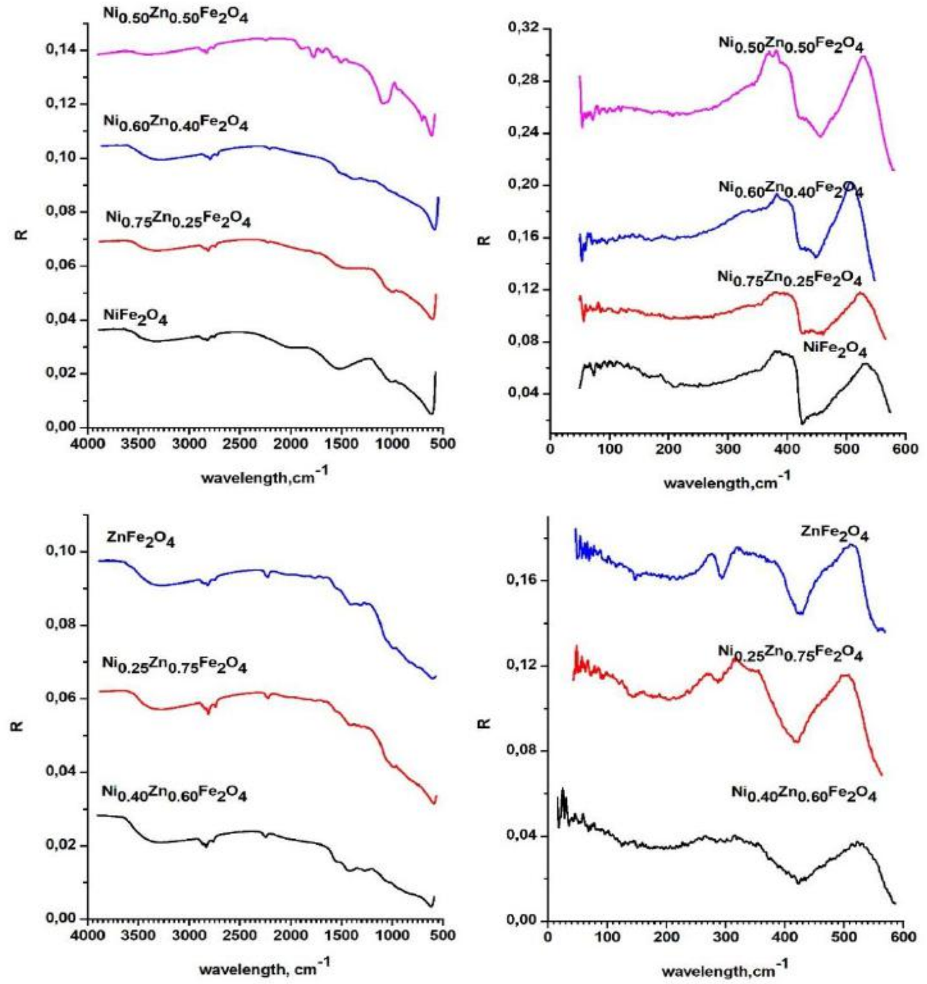

Fig. 1. Diffuse reflection IR spectra of $Ni_{1-x}Zn_xFe_2O_4$ ferrites in 4000-700cm^{-1} and in 600-50cm^{-1}.

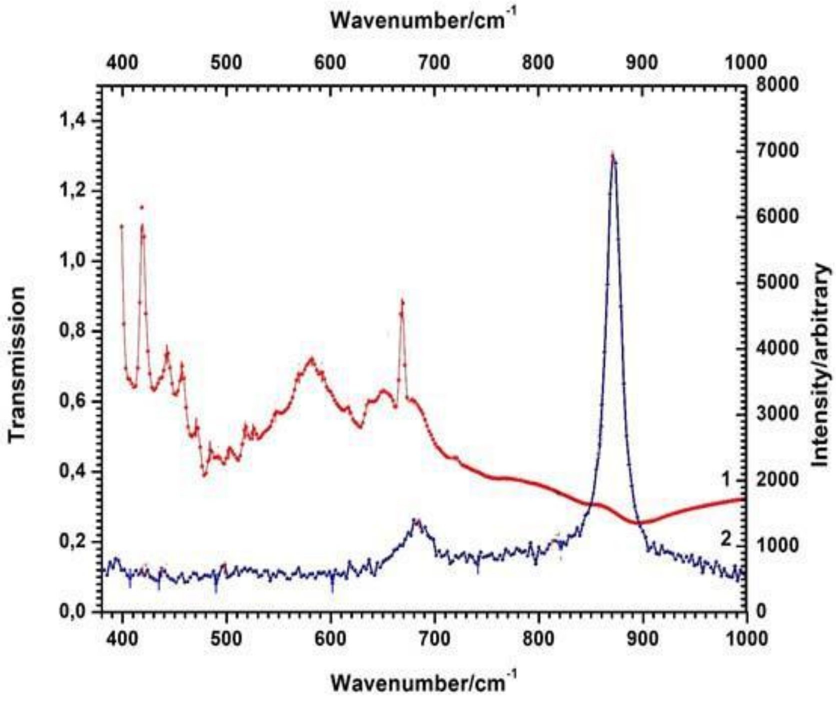

Fig. 2. The FTIR (1) transmission and Raman (2) spectra of $Ni_{0.4}Zn_{0.6}Fe_2O_4$ thin film.

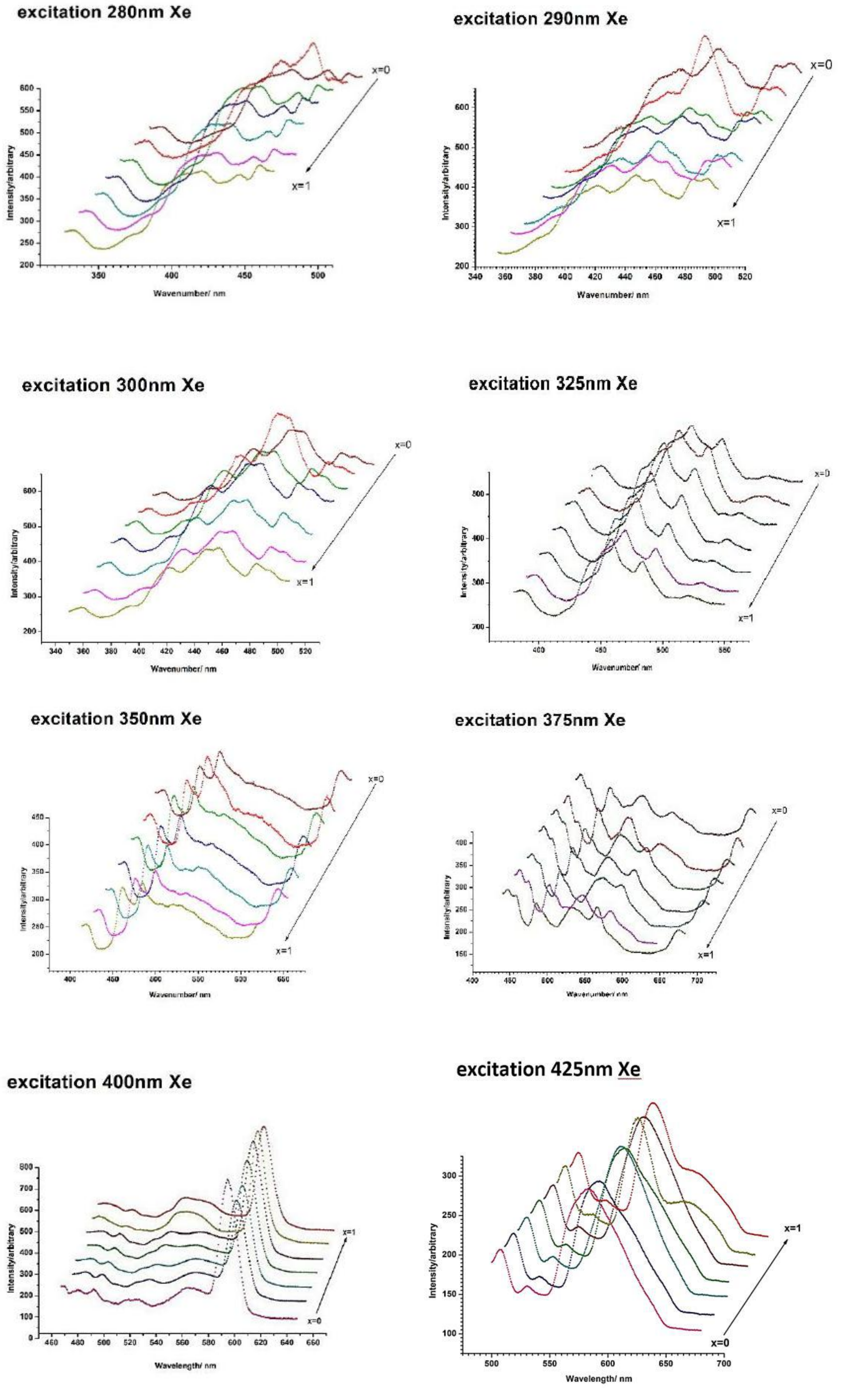

Fig. 3. Luminescent spectra of $Ni_{1-x}Zn_xFe_2O_4$ compositions.

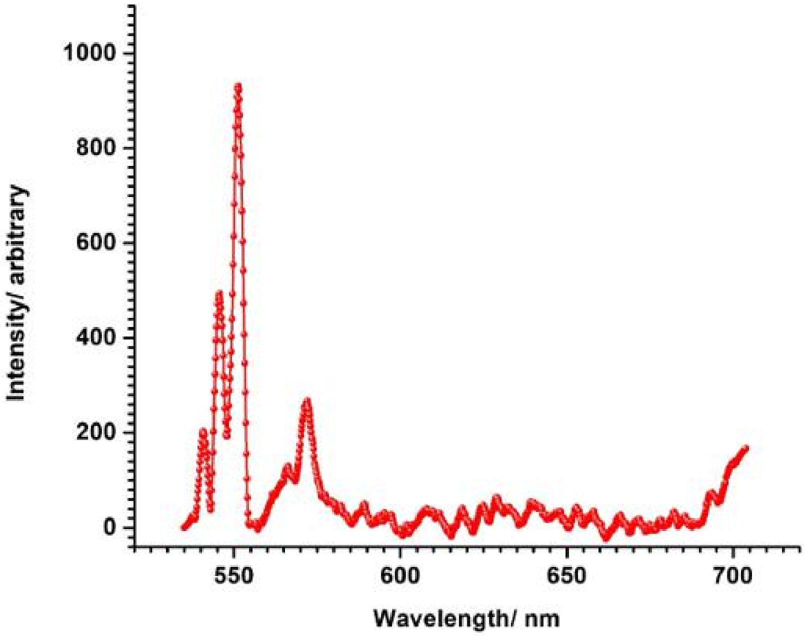

Fig. 4. The luminescent spectrum of $Ni_{0.4}Zn_{0.6}Fe_2O_4$ (excitation by of YAG Nd laser, λ = 532nm) with the radiation power of 5mW. The maxima correspond to: 540 nm, 545 nm, 551 nm, 566 nm, 572 nm.

Table 1.

The maxima of $Ni_{1-x}Zn_xFe_2O_4$ infrared spectra

Frequencies of *$Ni_{1-x}Zn_xFe_2O_4$* ferrites, cm^{-1}												
	[8]			[8]			[8]		[8],[15]			[8], [9]
x / symmetry	0	0	0.25	0.3	0.4	0.5	0.5	0.6	0.7	0.75	1.0	1.0
F_{1u}^1	604	604	592	590	584	578	578	582	571[8] 582[15]	570	-	569 [9]-
		-	-		-	544		544		550	542	542 [8]
		533	538		522			535		-	-	
		529	528		512	529		525		516	519	
		-	524		508	-		518		506	507	
		-	456		497	454		-		500	471	463 [8]
		443	442		437	436		-		-	-	
		432	433			429		430		-	-	
F_{1u}^2	426	425	426	426	426	424	426	-	426[8]	421	426	420 [9]
		-	403		401	-		403	401[15]	394	398	
		392	391		389	389		388		391	388	
		-	367		363	356		-		330	332	
		349	345		346	343		324		-	-	
		306	306		304	300		299		308	313	
		273	275		270	266		284		287	294	
F_{1u}^3		249	247		-	248		236		-	247	
		-	204		204	206		195		206	206	206 [8]
		169	169		171	173		163		177	183	
		96	93		95	95		128		81	84	
		95	90		89	88		55		77	80	
		-	85		84	83		52		73	76	
		74	76		71	72		43		58	69	

Table 2.

UV-Vis photoluminescence spectra of $NiFe_2O_4$

This work, nm	Some scientific publications											
	Luminescence, nm						**Optical absorption, nm**					
	$ZnFe_2O_4$ [9]	**$NiFe_2O_4$ [10,14]**	**Ni:ZnO[3*] $Ni_{1-x}Zn_xFe_2O_4$ [18]**	**NiO [4*]**	**Fe_3O_4 [5*], Fe_2O_3 Fe^{3+} in maghemite (m) and hematite (h) [19]**		**Fe^{3+} [15]**		**Fe^{2+} and Fe^{3+} [16]**		**Ni^{2+} [17]**	
332					315 (m) and 319 (h) [19]	$^6A_1 \rightarrow ^4T_1$	330	$^6A_{1g} \rightarrow ^4E(G)$			330	$^3A_{2g}(F) \rightarrow ^1T_{2g}(G)$
373	365	372 [10]		370	370 (m) [19]	$^6A_1 \rightarrow ^4E$			372	$^5E \rightarrow ^3E$ of $^TFe^{2+}$		
381				381	380 (h) [19]	$^6A_1 \rightarrow ^4E$	385	$^6A_{1g} \rightarrow ^4A_{1g}(G)$	385	$^5E \rightarrow ^3T_2$, $^3T_1$ of $^TFe^{2+}$	385	$^3A_{2g}(F) \rightarrow ^1T_{1g}(G)$
396	401			396	400 [13]				402	$^6A_{1g} \rightarrow ^4E_g$ of $^OFe^{3+}$	400	$^3A_{2g}(F) \rightarrow ^3T_{1g}(P)$
406				410	403 (m) and 405 (h) [19]	$^6A_1 \rightarrow ^4T_2$	410					
421	428	428 [14]										
448	454	441 [14]			434 (m) and 444 (h) [19]	$^6A_1 \rightarrow ^4E, ^4A_1$	440	$^6A_{1g} \rightarrow ^4T_{2g}(G)$				
462	468	459, 465 [14]	460[18]						459	$^6A_{1g} \rightarrow ^4A_{1g}$, ^4E_g of $^OFe^{3+}$	464	$^3A_{2g}(F) \rightarrow ^1T_{1g}(D)$
486		486 [10]	484[18]	481					477	$^6A_{1g} \rightarrow ^4A_{1g}$, ^4E_g of $^OFe^{3+}$		
496	494	496 [14]		490								
507		502 [14]		507	510 (m) [19]	$2^6A_1 \rightarrow 2^4T_1$						
521		530 [10]	518[18]		529 (h) [19]	$2^6A_1 \rightarrow 2^4T_1$	525	$^6A_{1g} \rightarrow ^4T_{1g}(G)$				
541 (R)			541[18]									
545(R)	539	535 [14]										
551(R)									555	$^5E \rightarrow ^3T_2$ of $^TFe^{2+}$		
559(R)												
566(R)			565 [11]		565 [3]							
571(R)												
597	593	594 [14]							588	$^5E \rightarrow ^3T_1$ of $^TFe^{2+}$		
606												
627							650	$^6A_{1g} \rightarrow ^4T_{1g}(G)$				
636					649 (h) [19]	$^6A_1 \rightarrow ^4T_2$			631	$^4A_2(F) \rightarrow ^4T_1(P)$		
673	665		660[18]		666 (m) [19]				670	$^OFe^{2+} \leftrightarrow ^OFe^{3+}$		

Here: From [17]: 642nm, 662nm, 682nm – tetrahedral (split); 656nm Fe^{3+} -tetrahedral; 682nm Fe^{2+} tetrahedral; 950nm - Fe^{2+} -octahedral and 2000nm - Fe^{2+} -tetrahedral [17] don't include to table; ^OFe -octahedral and ^TFe – tetrahedral iron cations; (D), (F), (G), (P) – terms of free ions. Luminescence maxima 540 nm, 545 nm, 551 nm, 566 nm, 572 nm of $Ni_{1-x}Zn_xFe_2O_4$ ferrites are interpreted as a consequence of the Raman effect [1].

The analysis of optical spectra of investigated compositions of $Ni_{1-x}Zn_xFe_2O_4$ ferrites in 4000cm^{-1}-500cm^{-1} range shows that the information about spectra of ZnO, NiO and Fe_2O_3 components is necessary for interpretation of spectral peculiarities. To identify the peculiarities of the optical reflection spectra of $Ni_{1-x}Zn_xFe_2O_4$ ferrites, the Kramers-Kronig procedure was used.

The transmission spectrum of $Ni_{0,4}Zn_{0,6}Fe_2O_4$ ferrite (fig. 2) was obtained on a thin film 40 nm thick in vacuum and is consistent with the diffuse reflectance spectrum of the nanopowder of this ferrite. The strong maximum observed in this composition of ferrite from the Raman spectrum is confirmed by the presence in the spectrum of its transmission of a very weak structure, which is explained by the prohibition by the rules of symmetry. Note that the following maxima were observed in this luminescence spectrum: 540 nm, 545 nm, 551 nm, 566 nm, 572 nm.

4.2 EXPERIMENTAL RESULTS OF LUMINESCENT INVESTIGATIONS

The luminescent spectra (Fig. 3-4) of synthesized $Ni_{1-x}Zn_xFe_2O_4$ compositions were studied at 300C from 300nm to 700nm and excited: 280 nm (4.427eV), 290 nm (4.275eV), 300 nm (4.132eV), 325 nm (3.814eV), 350 nm (3.542eV), 375 nm (3.306eV), 400nm (3.099eV), 425 nm (2.917eV) from the Xe-source and 532 nm (2.33eV) from the YAG Nd laser. The results are presented in Table 2. For the analysis of spectra, the procedure of decomposing into Gaussian components was used. Table 2 presents the comparison the positions of the luminescent maxima of $ZnFe_2O_4$ [9], $NiFe_2O_4$ [10,14], Ni:ZnO [11], $Ni_{1-x}Zn_xFe_2O_4$ [18], NiO [12] and Fe_3O_4 [13] compounds and maxima of optic absorption spectra [15-17].

4.3 DISCUSSION OF OPTICAL AND LUMINESCENT INVESTIGATIONS RESULTS

As follows from the group-theoretical representations, the infrared reflection spectra of $Ni_{1-x}Zn_xFe_2O_4$ three-fold degenerate symmetry modes F_{1u} should be observed. These oscillations are asymmetric with respect to the center of inversion and symmetric with respect to a second-order axis or vertical reflection planes (σ_v). Note that the masses of Fe, Ni and Zn elements, which are part of the studied ferrites, are much higher than the mass of the oxygen ion and, therefore, the oscillations of oxygen ions will have almost no effect on the positions of heavy ions, while, naturally, will affect the vibrations of the oxygen ion. The shift of the oxygen atom can occur either along the axis of the third order C_3, or perpendicular to it [20]. In the first case, the F_{1u}^1 bond is observed in $Me^{2+}-O-3Me^{3+}$ (where Me^{2+} is octahedral cation, $3Me^{3+}$-three tetrahedral cations). This oscillation corresponds to the high-frequency band of the spectrum. When oxygen is displaced perpendicular to the C_3 axis, F_{1u}^2 bonds $Me^{3+}-O-2Me^{3+}$ bonds are observed. This oscillation corresponds to the low-frequency band of the spectrum. The oscillations of cations relative to each other F_{1u}^3 (the bond $Me^{3+}-Me^{3+}$) of symmetry type occur at lower frequencies and have weak intensities. Note that during the processes of cation substitutions, the parameter "a" of the unit cell also changes. First of all, we note that the weakly intense, broad absorption band (3627-3500)cm^{-1} corresponds to the contribution from the $(OH)^-$ ions to the spectrum, the appearance of which indicates a high surface activity of ferrite microparticles due to the presence of dangling bonds and, as a result, to a high probability of adsorption by ions $(OH)^-$ and H^+ of active OH^- groups [21]. As was shown in [22], the presence of OH-groups allows magnetite nanoparticles, an analogue of $Ni_{1-x}ZnxFe_2O_4$ ferrites, to easily bind with polymeric compounds. The absorption band at 1630cm^{-1} was interpreted as deformation vibrations HOH, and at 823cm^{-1} and 1045cm^{-1} as deformation vibrations of the Zn–O–H and Fe–O–H bonds. The absorption bands in the frequency range with maxima around 430cm^{-1} and 542cm^{-1}, which are combined vibration bands of Fe–O valence bonds in octahedral positions with Zn^{2+} ions in the nearest coordination environment: Fe–O–Zn, are primarily, on the formation of a spinel structure. They can also be observed, for example, in $ZnFe_2O_4$.

As is well known, $Ni_{1-x}Zn_xFe_2O_4$ ferrites do not dissolve excessive amounts of NiO and ZnO. On the other hand, an excessive amount of Fe_2O_3 leads to the formation of a solid solution containing a mixture of $Ni_{1-x}Zn_xFe_2O_4$ and magnetite Fe_3O_4. Note also that in order to achieve a steady state, various forms of disorder in the form of point defects and vacancies always appear in spinel structures, the stability and concentration of which practically do not change until the thermodynamic equilibrium is violated. In the spectra of Fe_2O_3, the Fe –O bonds are represented by the characteristic doublet of the bands 545cm^{-1} and 470cm^{-1}, respectively F_{1u}^1 and F_{1u}^2 types of symmetry. In magnetite and nanomagnetite, similar doublets observed in (595 cm^{-1} and 415 cm^{-1}) and (590 cm^{-1} and 415 cm^{-1}) ranges. The doublet structure (590 cm^{-1} and 413 cm^{-1}) is also observed in ZnO micropowders. In the spectral band (530 cm^{-1} –430 cm^{-1}) there is a structure corresponding to the Ni-O bond in NiO. Comparison of the IR spectra of ZnO, NiO and Fe_2O_3 with the spectrum of $NiFe_2O_4$ makes it possible to interpret the doublet (604 cm^{-1} and 425 cm^{-1}) as oscillations of Ni-O and Fe-O bonds, respectively. As follows from Table 1, with an increase in "x" in the $Ni_{1-x}Zn_xFe_2O_4$ compositions, the line shifts to 604cm^{-1} towards 570 cm^{-1}; and in $ZnFe_2O_4$ it is recorded as a line of 542 cm^{-1} [23] or 569 cm^{-1} [24]. As is known, for the composition of magnetite Fe_3O_4, the positions of the IR spectrum lines are 624 cm^{-1}, 591 cm^{-1} and 425 cm^{-1} [25]. Note that the position of the 425 cm^{-1} line, interpreted as oscillations of the F_{1u}^2 type of symmetry, is practically independent of the change in "x" in $Ni_{1-x}Zn_xFe_2O_4$, which allows interpreting it as oscillations of Fe-O bonds, that is ($Fe^{3+}-O-2\,Fe^{3+}$).

The dependences of the intensities of the obtained IR spectra of the $Ni_{1-x}Zn_xFe_2O_4$ compositions under study were interpreted within the framework of a model that takes into account changes in the concentrations of Fe^{2+} [26] and Fe^{3+} cations [27] in ferrite compositions. As follows from the results obtained, a change in the concentrations of these cations with a change in "x" leads to changes in the intensity of the reflection spectra, the maximum of which is located near the composition x = 0.6. Near this composition, the difference in the concentration of Fe^{2+} cations decrease sharply and at x = 0.7 it becomes equal to the concentration of Fe^{3+} cations. A change in the concentrations of Fe^{2+} and Fe^{3+} cations in ferrite compositions indicates a change in the number of "jump" electrons in the superexchange interaction and, since these electrons, according to the model [28], form their "own" magnetic field, the change in their concentrations should affect the overall magnetic distribution fields in ferrite. This conclusion is confirmed by the EPR studies of the $Ni_{1-x}Zn_xFe_2O_4$ ferrites [4]. Correspondingly, the frequencies of the vibrational spectrum of the magnetic "subcoil" "jumping" electrons can to observe in the IR spectra of the ferrite compositions under study. This fact was also confirmed by studies of antiferromagnetic resonance in NiO: Fe^{2+} [29], in which the presence in the IR absorption spectrum at a temperature of 300K of the structure at 1600cm^{-1}, which coincides with the position of the two-magnetic zone previously detected in the Raman scattering spectra, was established. According to the authors of the publication, this structure has an impurity character. In our studies, in different $Ni_{1-x}Zn_xFe_2O_4$ compositions, the position of such a structure is found in the spectral band (1550-400)cm^{-1}, practically without changing its position. However, changes in the intensity of this spectral band are consistent with a model that takes into account changes in the concentrations of Fe^{2+} and Fe^{3+} cations in different $Ni_{1-x}Zn_xFe_2O_4$ compositions.

As shown in table 1, oscillations of the F_{1u}^3 type, occurring between like cations, are observed in the region of the far IR spectrum from 300cm^{-1} to 50 cm^{-1}. They correspond to the spectral lines 249 cm^{-1} ($NiFe_2O_4$), and 206 cm^{-1} ($ZnFe_2O_4$). The presence of a line at about 249 cm^{-1} in all compositions of $Ni_{1-x}Zn_xFe_2O_4$ indicates its belonging to vibrations $Fe^{3+}-Fe^{3+}$ bonds. Accordingly, the line 206 cm^{-1} is observed only in compositions in which Zn is present. An absorption maximum of 206cm^{-1} was observed in $ZnFe_2O_4$, also, for example, in [30]. The lines of antiferromagnetic resonance in NiO (36 cm^{-1}) [31] and Fe_2O_3 (10cm^{-1}) [32] are also located in this region. As follows from the results of [4], the presence of a magnetic field of "jumping" electrons [28] can lead to the appearance of antiferromagnetic resonance in $Ni_{1-x}Zn_xFe_2O_4$ ferrites, which is estimated to be in the region of ~ 2-3THz (70 cm^{-1}-100 cm^{-1}).

Note that the detected dependence of the intensity of the IR spectrum in different compositions $Ni_{1-x}Zn_xFe_2O_4$, consistent with the model of changes in cation concentrations, in particular, Fe^{2+} and Fe^{3+} (as well as Ni^{2+}, Ni^{3+}, Zn^{2+}), implicitly implies the presence of noticeable electron-phonon interaction and the effect impurity atoms in the formation of the IR spectrum of all compositions of ferrites, and, as mentioned above, point defects and vacancies always appear in order to achieve a steady state in spinel structures. Note that the shape of the spectrum of an impurity is related to the intensity of a set of electronic-vibrational transitions of the corresponding electronic transition of an impurity, and the shape of the vibronic satellite of a phononless line is determined by the states of the system in the initial and final states. In particular, theoretical studies [33] of the Ni^{3+} impurity charged with respect to the ZnO crystal lattice showed that the interaction of the impurity with the ions of the nearest environment leads to the appearance of a large number of additional maxima, among which resonant and gap oscillations were detected at frequencies of 8.2THz (273 cm^{-1}) and 11.2THz (373 cm^{-1}).

Photoluminescence spectroscopy is an important tool for the study of electronic and optical properties, in this case, $Ni_{1-x}Zn_xFe_2O_4$ ferrites, providing information on the structure of their forbidden zones, in the positions and states of defects and impurities. For completeness of information, the luminescence spectra were obtained at different excitation energies. Table 2 presents the comparison the positions of the luminescent [9-14, 18] and optic absorption spectra maxima [15-17]. Note that the photoluminescence maxima 540 nm, 545 nm, 551 nm, 566 nm, 572 nm of $Ni_{1-x}Zn_xFe_2O_4$ ferrites (fig. 3-4), observed upon excitation with the 532nm line from the YAG Nd laser, are interpreted as a consequence of the Raman effect, the study of which can be found in [1].

Characteristic, as indicated in [34] for the tetrahedral oxygen environment of the Fe^{3+} cation is the presence of absorption bands of about 435 nm and the absence of bands of 909 nm. In this case, the 448 nm luminescence band observed in our experiments in $Ni_{1-x}Zn_xFe_2O_4$ can be assigned to the $^6A_{1g} \leftarrow {}^4T_{2g}$ transition, the 407 nm band to the $^6A_{1g} \leftarrow {}^4T_{2g}$ transition, and 373 nm to the degenerate transitions: $^6A_{1g} \leftarrow {}^4A_{1g}$ и $^6A_{1g} \leftarrow {}^4E$.

The UV- V is photoluminescence spectra of $NiFe_2O_4$ were obtained upon excitation by the 325 nm line. It can be noted that the observed violet maxima at 372 nm, 420 nm, the blue band at 486 nm and the green band at 530 nm are quite consistent and interpreted with the published absorption and luminescence spectra (see table 2).

Radiation from the violet region, as indicated in [35], arises due to transitions of electrons from the shallow donor level to the valence band. Blue radiation was attributed to free and bound excitons at the band boundary [36]. In addition, it is generated by electronic transitions from the near conduction band to acceptors of deep levels and transitions from deep donor levels to the valence band [37]. The green 530 nm band of radiation refers to an oxygen vacancy with other defects associated with the vacancy [38].

Physically, the basis of the $Ni_{1-x}Zn_xFe_2O_4$ photoluminescent spectra interpretation was the conclusions of the crystal field theory [39-41and other]. In crystalline fields of tetrahedral and octahedral symmetries, the fivefold degenerate 6S level of the 3d5 electrons of the Fe3+ cation is split into two energy levels, separated by an energy gap of 10Dq (fig.5). The type of splitting is determined by the symmetry of the environment with O2– anions. The splitting of the transition metal ion levels in an octahedrally coordinated crystal field is opposite to the tetrahedral field, that is, with a higher doublet eg and lower triplet *t2g.*

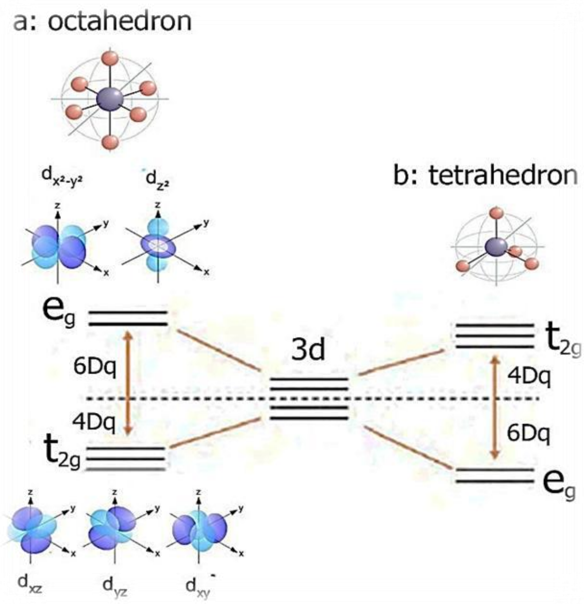

Fig. 5. (a) octahedral and (b) tetrahedral symmetry. In the crystal field, the 3d5 orbital splits into doublet e_g, and triplet t_{2g} levels. The amount of splitting between levels is 10 Dq.

a. octahedral symmetries: the doubly degenerate eg level and the triple degenerate t2g level form a high-spin electron configuration (t2g)3↑(eg)2↑ with an effective spin of 5/2. Crystal field stabilization energy (CFSE) for electrons t_{2g} and eg:

$$(CFSE)=3\times(-0.4\Delta_{oct})+2\times(0.6\Delta_{oct})=0$$

b. The (CFSE) for low-spin electron configuration (t2g)5↑(eg)0↑:5×(-0.4Δ_{oct})+2P=-2Δoct+2P, where 2P is pairing energy term
c. For Fe^{2+} cation (d6 ion) in a spherical crystal field, one d orbital contains spin-paired electrons and four orbitals is singly occupied. The high-spin electron configuration in octahedral field is (t2g)4↑(eg)2↑ and (CFSE)=-0.4Δ_{oct}. For a low-spin d6 electron configuration (t2g)6↑(eg) 0↑ (CFSE) =-2.4Δ_{oct} +2P
d. For Ni^{2+} cation (d8 ion) in a spherical crystal field, d orbital contains three spin-paired electrons and two orbitals is singly occupied. The high-spin electron configuration in octahedral field is (t2g)6↑(eg)2↑ and (CFSE)=-1,2Δ_{oct}
e. For Zn^{2+} cation (d10 ion) in a spherical crystal field, d orbital is full and (CFSE)=0

Additional splitting of the eg and t2g levels can occur as a result of tetragonal, trigonal, or orthorhombic distortions of tetrahedrons and octahedra [42], and these levels are filled with electrons in accordance with the Hund rule. According to the Jahn – Teller theorem (JT), in the ground state only spin degeneracy is allowed, and all other degeneracy is removed with small distortions of the octahedra or tetrahedra, which reduce the symmetry of the crystal [43]. Then: for d5, a weak low-spin JT is observed; for d6 - weak high-spin JT; for d8 - not JT effect expected.

For a regular tetrahedron, the splitting of the d orbitals is inverted compared with that for a regular octahedral structure, and the energy difference Δ_{tet} is smaller. The relative splittings: $\Delta_{tet} = 4/9\Delta_{oct}$. As well known, tetrahedral complexes are almost invariably high-spin. Only a strong field ligand which lowers the symmetry of the complex can lead to a low-spin ‘distorted tetrahedral’ system.

CONCLUSION

The optical and luminescent spectra of $Ni_{1-x}Zn_xFe_2O_4$ ferrite nanopowders with x=0;0,25;0,4;0,5; 0,6;0,75;1,0 were investigated in 4000-50 cm^{-1} and 200-700nm at room temperature. The agreement with the data of published studies of other authors allowed us to give a hypothetical interpretation of the results.

ACKNOWLEDGEMENTS

The present work is supported by Science Development Foundation under the President of the Republic of Azerbaijan (grant № EIF-BGM-3-BRFTF- 2+/ 2017-15/04/1 and grant № EİF-2013-9(15)-46/05/1).

[1] *S. Aliyeva, S. Babayev, T. Mehdiyev.* Raman spectra of $Ni_{1-x}Zn_xFe_2O_4$ nanopowders, *JRS* 2018; 49 (2), 271.

[2] *Sh.N. Aliyeva, A.M.Kerimova, R.B. Abdullayev, T.R. Mehdiyev.* IR spectra of $Ni_{1-x}Zn_xFe_2O_4$ ferrite micropowders, PhSS, 2017, v. 59, no. 3, pp. 528 – 533.

[3] *Sh.N. Aliyeva.* Magnetic properties of $Ni_{1-x}Zn_xFe_2O_4$ micropowders and thin films, Baku, 2017, p. 199.

[4] *Sh.N. Aliyeva, Y.N. Aliyeva, A.I. Nadjafov, I.S. Hasanov, E.K. Huseynov T.R. Mehdiyev.* EPR and SPM studies of Zn-Ni ferrites, Phys. Status Sol. (c), 615, 2015/DOI 10.1002/ pssc.201400273.

[5] *N.N. Scholtz, K.A. Piskarev.* Ferrimagnetic materials for radio-frequencies, Publishing House Energy, Moscow, 2013.

[6] *U.V. Kasyuk, L.A. Bliznyuk, N.A. Basov, A.K.Fedotov, A.S. Fedotov, I.A. Svito.* Structure and electro-physical properties of doped ceramics on the base of zinc oxide. The theses of International conference, Minsk, November 22 – 25, 2016, vol. 2, pp. 84-86.

[7] *J. Nishitani, K. Kozuki, T. Nagashima, M. Hangyo.* Appl.Phys. Lett.2010,96,221906-1.

[8] *F.Sh. Tehrani, V. Daadmehr, A.T. Rezakhani, R.H. Akbarnejad, S. Gholipour.* J. Supercond. Novel Magnetism, 2012, 25, 2443.

[9] *R.C. Sripriya, Ezhil Arasi S. Madhavan. J. Victor Antony Raj M.* Synthesis and Characterization studies of $ZnFe_2O_4$ nanoparticles, MMSE Journal vol.9, iss.1, 2017, p.13-18.

[10] *K. Kombaiah, J. Judith Vijaya∗, L. John Kennedy, K. Kaviyarasu.* Catalytic studies of $NiFe_2O_4$ nanoparticles prepared by conventional and microwave combustion method, Materials Chemistry and Physics 221, 2019, 11–28.

[11] *Jamil K. Salem, Talaat M. Hammad, Roger R. Harrison.* Synthesis, structural and optical properties of Ni-doped ZnO micro-spheres, J Mater Sci: Mater Electron, 2012, DOI 10.1007/s10854-012-0994-0.

[12] *P.A. Sheena, K.P. Priyanka, N. Aloysius Sabu, Boby Sabu, Thomas Varghese.* Effect of calcination temperature on the structural and optical properties of nickel oxide nanoparticles, Nanosystems: Physics, Chemistry, Mathematics, 2014, 5 (3), p.441-449.

[13] M.E. Sadat, Masoud Kaveh Baghbador, Andrew W. Dunn, H.P. Wagner, Rodney C. Ewing, Jiaming Zhang, Hong Xu, Giovanni M. Pauletti, David B. Mast and *Donglu Shi.* Photoluminescence and photothermal effect of Fe_3O_4 nanoparticles for medical imaging and therapy, Applied Physics Letter, 105, 0919031-091903-5, 2014.

[14] *Walmir E. Pottker, Rodrigo Ono, Miguel Angel Cobos, Antonio Hernando, Jefferson F.D.F. Araujo, Antonio C.O. Bruno, Sidney A. Lourençoa, Elson Longo, Felipe A. La Porta.* Influence of order-disorder effects on the magnetic and optical properties of $NiFe_2O_4$ nanoparticles, 44, 2018, 17290–17297.

[15] *S. Lakshmi Reddy, Tamio Endo and G. Siva Reddy.* Electronic (Absorption) Spectra of 3d Transition Metal Complexes, in book IntechOpen: Advanced Aspects of Spectroscopy, chapter 1, 2012.

[16] *Veronica D'Ippolito, Giovanni Battista Andreozzi, Ulf Hålenius, Henrik Skogby, Kathrin Hametner, Detlef Günther.* Color mechanisms in spinel: cobalt and iron interplay for the blue color, Phys Chem Minerals, 2015, 42:431–439.

[17] *H.K. Mao and P.M. Bell.* Crystal-field effects in spinel: oxidation states of iron and chromium, Geochimica et Cosmochimiea Aeta, 1975, vol. 39, pp. 869 to 871.

[18] *F. Shahbaz Tehrani, V. Daadmehr, A.T. Rezakhani, R. Hosseini Akbarnejad, S. Gholipour.* Structural, magnetic, and optical properties of zinc- and copper- substituted nickel ferrite nanocrystals Journal of Superconductivity and Novel Magnetism, 2012, vol. 25, issue 7, pp 2443-2455, DOI:10.1007/s10948-012-1655-5.

[19] *David M. Sherman and T. David Waite.* Electronic spectra of Fe^{3+} oxides and oxide hydroxidesin the near IR to near UV, American Mineralogist, vol. 70, p. 1262-1269, 1985.

[20] The Infrared Spectra of Minerals**,** 539 pp., Mineral**.**Soc., London**,** 1974.

[21] *J.T. Keiser, C.W. Brown, R.H. Heidersbach.* Infrared spectra of magnetite nanoparticles, J. Electrochem. Soc. 1982, vol. 129, p. 2686.

[22] *Ma M., Zhang Yu., Wei Yu. et. al.* Preparation and characterization of magnetite nanoparticles coated by amino silane, Colloids and Surfaces: Physicochem. Eng. Aspects. 2003, vol.212, p.219-226.

[23] *F. Shahbaz Tehrani, V. Daadmehr, A.T. Rezakhani, R. Hosseini Akbarnejad, S. Gholipour.* Structural, magnetic, and optical properties of zinc- and copper- substituted nickel ferrite nanocrystals Journal of Superconductivity and Novel Magnetism, 2012, vol. 25, issue 7, pp 2443-2455, DOI:10.1007/s10948-012-1655-5.

[24] *Jiaqi Wan, Xuehui Jiang, Hui Li and Kezheng Chen.* Facile synthesis of zinc ferrite nanoparticles as non-lanthanide T1 MRI contrast agents, Journal of Material Chemistry, 2012, 22, 13500-13505.

[25] *Zahra Rezay Marand, Mitra Helmi Rashid Farimani, Nasser Shahtahmasebi.* Study of magnetic and structural and optical properties of Zn doped Fe3O4 nanoparticles synthesized by co-precipitation method for biomedical application, Nanomedicine Journal, v. 1, no. 4, 2014, p. 238-247.

[26] *Santosh S. Jadhav, Sagar E. Shirsath, B.G. Toksha, S. J. Shukla, K. M. Jadhav.* Effect of Cation Proportion on the Structural and

Magnetic Properties of Ni-Zn Ferrites Nano-Size Particles Prepared By Co-Precipitation Technique, Chinese Journal of Chemical Physics, vol.21, N4, 2008, p.381-386.

[27] *F. Shahbaz Tehrani, V. Daadmehr, A.T. Rezakhani, R. Hosseini Akbarnejad, S. Gholipour*. Structural, magnetic, and optical properties of zinc- and copper- substituted nickel ferrite nanocrystals Journal of Superconductivity and Novel Magnetism, 2012, vol. 25, issue 7, pp 2443-2455, DOI:10.1007/s10948-012-1655-5.

[28] *K.P.Belov*. Ferrimagnets with "weak" magnetic sublattice, UFN, 1996, June, vol. 166, no. 6, pp. 669 – 681.

[29] *C.R. Becker, Ph. LAU, R.Geick* and *V. Wagner*. Antiferromagnetic Resonance in NiO:Co^{2+} and NiO :Fe^{2+}, Phys.Stat.Sol. (b) 67, 653-663 1975.

[30] *Vidales J.L. M., A.L. Delgado, E. Vila* and *F.A. Lopez.* The effect of the starting solution on the physico-chemical properties of zinc ferrite synthesized at low temperature, J. Alloys Comp., 1999, 287, 276.

[31] *Junichi Nishitani, Kohei Kozuki, Takeshi Nagashima* and *Masanori Hangyo*. Terahertz radiation from coherent antiferromagnetic magnons excited by femtosecond laser pulses, Appl. Phys. Lett.,96, p. 221906-1-221906-3, 2010.

[32] *Shin G. Chou, Paul E. Stutzman, Shuangzhen Wang, Edward J. Garboczi, William F. Egelhoff, and David F. Plusquellic*. High-Resolution Terahertz Optical Absorption Study of the Antiferromagnetic Resonance Transition in Hematite (α-Fe_2O_3), J. Phys. Chem. *C*, 2012, 116 (30), p.16161–16166.

[33] *A.N. Kislov, V.G. Mazurenko, A.N. Varaksin*. Analysis of vibronic structure of optical spectra in ZnO:Ni^{+3} crystals on the base of localized oscillation modelling, Phys. Stat. Sol, 1999, vol. 4, pp. 618 – 622.

[34] *A.B.P. Lever.* Inorganic Electronic Spectroscopy. Amsterdam: Elsevier, 1968; *D.M. Sherman, T.D. Waite.* Electronic spectra of Fe^{3+} oxides and oxide hydroxides in the near IR to near UV, Amer. Mineralogist. 1985, 70, p. 1262.

[35] *A.V.Dijken, E.AMeulenkamp,D.Vanmaelbergh, A. Meijerink.* The Kinetics of the radiative and nonradiative processes in nanocrystalline ZnO particles upon photoexcitation, J. Phys. Chem. B 104, 2000, 1715-1723.

[36] *L.Jing, Y. Qu, B. Wang, S. Li, B. Jiang, L.Yang, W.Fu, H.Fu.* Review of photoluminescence performance of nano-sized semiconductor materials and its relationships with photocatalytic activity, J. Sun, Sol. Energy Mater. Sol. Cells 90, 2006, 1773-1787.

[37] *R.K. Sendi, S. Mahmudm,* Quantum size effect on ZnO nanoparticle-based discs synthesized by mechanical milling, Appl. Surf Sci. 258, 2012, 8026–803.1.

[38] *J. Becker, K.R. Raghupathi, J. St Pierre, D. Zhao, R.T. Koodal.* Tuning of the crystallite and particle sizes of ZnO nanocrystalline materials in solvothermal synthesis and their photocatalytic activity for dye degradation, J. Phys. Chem. C 115, 2011, 13844-13850

[39] *D.I. Khomskii.* Transition metal oxides. Cambridge University Press, Cambridge, 2014. ISBN: 978-1-107-02017-7.

[40] *Burns, Roger G. Mineralogical*. Applications of Crystal Field Theory, ISBN 10: 0521076102/ISBN 13: 9780521076104, Published by Cambridge University Press, Cambridge, 1970.

[41] *E. Pavarini, E.Koch, F.Anders.* Correlated Electrons: From Models to Materials, Crystal-field Theory, Tight-binding Method, and Jahn-Teller Effect Julich 2012, ISBN 978-3-89336-796-2.

[42] *D.I. Khomskii.* Transition metal oxides. Cambridge University Press, Cambriage, 2014. ISBN: 978-1-107-02017-7.

[43] *I.B. Bersuker.* The Jahn-Teller Effect. Cambriage University Press, Cambridge, 2006. ISBN 139780521822121.

Received: 06.09.2019